Published in final edited form as:

Nanotoxicology. 2020 March ; 14(2): 145–161. doi:10.1080/17435390.2019.1668067.

Defect-Induced Electronic States Amplify the Cellular Toxicity of ZnO Nanoparticles

Indushekhar Persaud[1], **Achyut J. Raghavendra**[2,3], **Archini Paruthi**[1,4], **Nasser B. Alsaleh**[1], **Valerie C. Minarchick**[1], **James R. Roede**[1], **Ramakrishna Podila**[2,3], **Jared M. Brown**[1]

[1]Colorado Center for Nanomedicine and Nanosafety, Department of Pharmaceutical Sciences, Skaggs School of Pharmacy and Pharmaceutical Sciences, University of Colorado Anschutz Medical Campus, Aurora, CO 80045, USA

[2]Department of Physics and Astronomy, Clemson University, Clemson, SC 29634, USA

[3]Clemson Nanomaterials Center and COMSET, Clemson University, Anderson, SC 29625, USA

[4]Materials Science and Engineering, Indian Institute of Technology, Gandhinagar, Gujarat, 382355, IN

Abstract

Zinc oxide nanoparticles (ZnO NPs) are used in numerous applications, including sunscreens, cosmetics, textiles, and electrical devices. Increased consumer and occupational exposure to ZnO NPs potentially poses a risk for toxicity. While many studies have examined the toxicity of ZnO NPs, little is known regarding the toxicological impact of inherent defects arising from batch-to-batch variations. It was hypothesized the presence of varying chemical defects in ZnO NPs will contribute to cellular toxicity in rat aortic endothelial cells (RAECs). Pristine and defected ZnO NPs (oxidized, reduced and annealed) were prepared and assessed three major cellular outcomes; cytotoxicity/apoptosis, reactive oxygen species production and oxidative stress, and endoplasmic reticulum (ER) stress. ZnO NPs chemical defects were confirmed by X-ray photoelectron spectroscopy and photoluminescence. Increased toxicity was observed in defected ZnO NPs compared to the pristine NPs as measured by cell viability, ER stress, and glutathione redox potential. It was determined that ZnO NPs induced ER stress through the PERK pathway. Taken together, these results demonstrate a previously unrecognized contribution of chemical defects to the toxicity of ZnO NPs, which should be considered in the risk assessment of engineered nanomaterials.

Keywords

nanotoxicity; defects; electronic states; zinc oxide; endothelial cell

Corresponding Authors: Jared M. Brown Ph.D., Department of Pharmaceutical Sciences, Skaggs School of Pharmacy and Pharmaceutical Sciences, University of Colorado Anschutz Medical Campus, 12850 E Montview Blvd, Aurora, CO 80045, United States of America, jared.brown@cuanschutz.edu, Ramakrishna Podila Ph.D., Department of Physics and Astronomy, Clemson Nanomaterials Center and COMSET, Clemson University, Clemson, SC 29634, United States of America, rpodila@g.clemson.edu.

***Disclosure of interest*:** Authors listed in the publication do not have any conflict of interest or benefited financially.

1. Introduction

Nanoparticles (NPs) are increasingly used in all aspects of society, but have also been recognized as a potential health risk. Zinc oxide (ZnO) NPs are commonly used in sunscreens, ceramics, plastics, glass, cement paints, adhesives, cosmetics, paints, semiconductors, rubber production, and medical applications among others (Klingshirn, 2007, Roth, Webb and Williams, 1982, Hong, Tripathy, Son, Ha, Jeong and Hahn, 2013, Zhang, Nayak, Hong and Cai, 2013). Specifically, ZnO NPs have been widely used due to their ability to protect against ultraviolet (UV) radiation, their wide band gap, and their ability to enhance the activity of antimicrobial compounds. The electrical applications take advantage of the wide band gap of ZnO NPs (3.37 eV) for the customization of varistors and semiconductors (Djurisic, Leung, Tam, Hsu, Ding, Ge, Zhong, Wong, Chan, Tam, Cheah, Kwok and Phillips, 2007). Some current and developing medical applications of ZnO include bioimaging, drug delivery, gene delivery, and biosensors (glucose, phenol, H_2O_2, cholesterol, urea) (Zhang, Nayak, Hong and Cai, 2013, Raghavendra, Gregory, Slonecki, Dong, Persaud, Brown, Bruce and Podila, 2018). Consumer applications of ZnO NPs include sunscreens due to their ability to block ultraviolet A and B bands (Smijs and Pavel, 2011). Due to the favorable properties and widespread use of ZnO NPs, human exposure during production, consumer use and medical applications are all areas of concern. Lastly, ZnO NP toxicity has been established both *in vitro* and *in vivo*; however, the mechanisms involved in toxicity and the contributions of their physicochemical properties have not been definitively determined (Hong, Tripathy, Son, Ha, Jeong and Hahn, 2013, Vandebriel and De Jong, 2012, Yu, Yoon, Minai-Tehrani, Kim, Park, Jeong, Ha, Lee, Kim and Cho, 2013, Sharma, Singh, Pandey and Dhawan, 2012).

In vitro and *in vivo* studies of ZnO NPs have demonstrated a number of different toxicological outcomes (Vandebriel and De Jong, 2012, Zhang, Ji, Xia, Meng, Low-Kam, Liu, Pokhrel, Lin, Wang, Liao, Wang, Li, Rallo, Damoiseaux, Telesca, Mädler, Cohen, Zink and Nel, 2012, Xia, Zhao, Sager, George, Pokhrel, Li, Schoenfeld, Meng, Lin, Wang, Wang, Ji, Zink, Madler, Castranova, Lin and Nel, 2011, Warheit, Sayes and Reed, 2009, Sayes, Reed and Warheit, 2007, Cho, Duffin, Poland, Howie, MacNee, Bradley, Megson and Donaldson, 2010, Cho, Duffin, Poland, Duschl, Oostingh, Macnee, Bradley, Megson and Donaldson, 2012). For example, ZnO NPs induce apoptosis in dermal fibroblasts (Meyer, Rajanahalli, Ahamed, Rowe and Hong, 2011). Previous studies have also demonstrated that the toxicity of ZnO NPs is associated with the immune system. For example, Xia *et al.* found macrophages exposed to ZnO NPs resulted in significant oxidative stress (Xia, Kovochich, Liong, Madler, Gilbert, Shi, Yeh, Zink and Nel, 2008). Similarly, oral exposure to ZnO NPs in mice resulted in oxidative stress, DNA damage, and apoptosis in the liver (Sharma, Singh, Pandey and Dhawan, 2012). In addition, it has been demonstrated that ZnO NPs induce endoplasmic reticulum (ER) stress in endothelial (HUVEC) and epithelial (CHO) cells (Chen, Huo, Shi, Bai, Zhang, Zhao, Chang and Chen, 2014). Further, it has been reported that mice exposed to ZnO NPs had an induction of ER stress in the liver (Yang, Shao, Liu, Gu, Shu, Mo, Chen, Zhang and Jiang, 2015). Overall, these studies indicate that ZnO NPs induce cellular stress often resulting in toxicity.

Gleaning the adverse physiological effects from different studies as discussed above, the identification of the most relevant physicochemical properties of engineered nanomaterial (ENMs) to predict the possible toxic effects has been one of the major focus areas in nanotoxicity. To this end, some theoretical frameworks that predict toxicity based on ENM physicochemical descriptors have been proposed (Zhang, Ji, Xia, Meng, Low-Kam, Liu, Pokhrel, Lin, Wang, Liao, Wang, Li, Rallo, Damoiseaux, Telesca, Mädler, Cohen, Zink and Nel, 2012, Puzyn, Rasulev, Gajewicz, Hu, Dasari, Michalkova, Hwang, Toropov, Leszczynska and Leszczynski, 2011, Burello and Worth, 2011). Relevant to metal-oxide ENMs, such as ZnO NPs, Burello and Worth (Burello and Worth, 2011) proposed that electrons could be transferred between ENMs and cellular redox species depending upon the electronegativity, ionization potential, or semiconductor band gap energy between valence (E_V) and conduction (E_C) bands. In this model, the electron transfer occurs only when the molecular energy levels of cellular redox species (as gauged by intracellular redox potential or IRP) overlap with ENM energy bands (viz., E_C or E_V), which could ultimately produce reactive oxygen species (ROS) and reactive nitrogen species (RNS) on the ENM surface. Building on this model, Zhang *et al.* proposed a predictive model for oxide ENMs using E_c and metal dissolution characteristics (Zhang, Ji, Xia, Meng, Low-Kam, Liu, Pokhrel, Lin, Wang, Liao, Wang, Li, Rallo, Damoiseaux, Telesca, Mädler, Cohen, Zink and Nel, 2012). While these models may help explain the toxicity of some ENMs, they fail to predict: i) batch-to-batch variations in ROS production for the same ENM (e.g., ZnO NPs) and ii) the toxicity of ENMs where there is no metal dissolution or overlap between IRP and the ENM energy bands. We hypothesized that the main reason for the failure of these models lies in the fact that they do not consider perhaps the most important characteristic of ENMs viz., the presence of defect-induced surface electronic states in addition to E_C and E_V.

From entropic considerations, defects are inadvertently produced during ENM synthesis. The scale-up of synthesis methods results in batch-to-batch variations in defects, which in turn elicit varying physical properties and different toxic responses. For example, the presence of different types of defects in ZnO NPs may result in significant changes in Zn dissolution and interactions of the ZnO NPs with biological systems such as protein binding and generation of ROS. Therefore, based on our previous studies on ENM-protein corona formation in which we demonstrated that physicochemical properties including surface functional groups and shape alter which proteins bind and which proteins change conformation, we hypothesized that the presence of varying chemical defects, which will alter charge transfer between proteins and ZnO NPs will contribute to cellular toxicity and stress (Shannahan, Lai, Ke, Podila, Brown and Witzmann, 2013, Podila, Chen, Ke, Brown and Rao, 2012, Podila, Vedantam, Ke, Brown and Rao, 2012, Raghavendra, Alsaleh, Brown and Podila, 2017).

To test this hypothesis, we examined three common cellular outcomes of NP exposure including cell viability, endoplasmic reticulum (ER) stress and oxidative stress in rat aortic endothelial cells (RAEC) exposed to ZnO NPs with different chemical defects. To address the role of NP chemical defects and their contribution to toxicity, we synthesized ZnO NPs with a consistent band gap and similar dissolution rates but introduced different chemical defects into the crystalline structure of the NP. Three different types of defects (viz., O-vacancies, Zn/O-interstitials, Zn-vacancies) were incorporated by subjecting the ZnO NPs to

annealing, oxidizing or reducing conditions, and compared their properties to that of pristine or as-prepared ZnO NPs. From our study, we demonstrated that the presence of chemical defects in ZnO NPs influences cellular uptake, viability, glutathione redox potential and induction of ER stress.

2. Materials and methods

2.1. Synthesis of ZnO nanoparticles with chemical defects

ZnO NPs were synthesized using a solvothermal technique. Briefly, zinc acetate dihydrate and polyvinylpyrrolidone (PVP, 10,000 g/mol) were dissolved in diethyleneglycol (DEG) and heated slowly to 180 °C. De-ionized water was then injected into hot zinc acetate-dissolved DEG solution using a syringe pump at a constant rate of 1 ml/s to induce nucleation of ZnO NPs. The reaction was stopped when the solution turned milky white upon the formation of ZnO NPs. Finally, NPs were separated from the liquid by centrifugation (10k rpm) and then washed repeatedly with methanol to remove PVP and DEG. Subsequent DI-water washing and centrifugation (10k rpm) was used to obtain ZnO NP powder or resuspend ZnO NPs in DI water. For annealing, the NP powders were loaded into a ceramic boat and inserted into a quartz tube (1” diameter) with a temperature of 500 °C for 1 hr. Different gas environments were used to obtain annealed (Ar), oxidized (O_2), or reduced (H_2) ZnO NPs with different defects. For annealed nanoparticles, the NPs were annealed in 500 sccm of Ar at 500 °C for one hour.

2.2. Characterization of ZnO nanoparticles

The ZnO NPs were suspended in water and DMEM/F12 (Corning, Corning, NY) and the hydrodynamic size and zeta potential were measured using a Zetasizer Nano ZS (Malvern, UK). The zeta potential was measured in dH_2O at a concentration of 10 μg/mL. Due to the ionic concentration of DMEM, we were not able to obtain an accurate measurement of zeta potential in this medium (see Table 1). Particle size was also measured by imaging the NPs using a Hitachi H-7600 transmission electron microscope at 100kV and using ImageJ software (NIH) to calculate the diameter of each particle (see supplementary information).

The dissolution of ZnO NPs (20μg/mL) under different biologically relevant media was quantified by using dialysis membrane (MWCO=3.5 kDa). The dialysis bags were loaded with 10mL ZnO NP suspension and were dialyzed across the given media (de-ionized water, artificial lysosomal fluid and cell culture media (DMEM)) of interest for the separation of released ions. The study was performed under dynamic conditions at 200rpm at 37°C for biologically relevant media and at 25°C for de-ionized water. The recovery of the system was evaluated by suspending 20μg/mL of Zn^{2+} ions instead of nanoparticles. 1mL aliquot was withdrawn from the setup at specific time points and was digested in 1%HNO_3. The concentration of Zn^{2+} ions was quantified through ICP-MS (NexION 2000, Perkin Elmer) under standard mode with 1ppb indium as the internal standard. The quantification was performed in duplicates (n=2) with a calibration plot of $R^2 = 0.9919$ (LOD=13ppt).

The chemical defects were examined by X-ray photoemission spectroscopy (XPS) using a Kratos Axis Ultra DLD instrument and spectra were calibrated by C 1s at 284.6 eV and

photoluminescence (PL) spectroscopy using a Horiba-Jobin Yvon Nanolog spectrophotometer with a Triax 550 monochromator with a liquid nitrogen cooled CCD detector. For PL, an excitation wavelength of 325 nm (corresponding to 3.8 eV) and emission was recorded between 1.6 and 3.4 eV to indicate the presence of chemical defects and band gap of the ZnO NPs.

2.3. Cell culture and cell viability

Rat aortic endothelial cells (RAEC) and rat endothelial cell growth media were purchased from Cell Applications, Inc. (San Diego, CA, USA). Cells were cultured under standard conditions of 5% CO_2 and 37 °C. After reaching 80% confluency, the cells were trypsinized and seeded for the studies.

RAECs were exposed to 5, 10, 15, 20, and 25 μg/mL of pristine, annealed, oxidized or reduced ZnO NPs for 24 and 48 hrs in 96 well plates and cell viability was tested. After the exposure, the media was removed and cells were washed with warm PBS and aspirated. Phenol red free DMEM/F12 (Hyclone, Utah, USA) was added to each well. A CellTiter 96® Aqueous One Solution Proliferation Assay (Thermo Fisher Scientific, MA, USA) MTS assay was used to measure cell viability. 10 μl of CellTiter was added to each well and the plates were incubated for 45 minutes. The optical density was measured at 490 nm with a Biotek Synergy HT microplate reader (Winooski, VT, USA). The percentage viability was calculated in comparison to control cells, which represent 100% viability. Additionally, cell viability was examined using Annexin V and propidium iodide staining. To this end, following the same treatment protocol as above, cells were washed with PBS twice and resuspended in 3 μM propidium iodide in PBS. Annexin V reagent (5 μl, BD Biosciences, San Jose, CA, USA) was added per sample and incubated for 15min at room temperature. Using an Accuri™ C6 flow cytometry (BD Biosciences, USA) fluorescence for both stains were analyzed for a minimum of 10,000 cells.

2.4. Cellular uptake of ZnO nanoparticles

RAECs were cultured as described above and exposed to 20 μg/mL of pristine, annealed, oxidized or reduced ZnO NPs for 6, 12, and 24 h. After the exposure, the cells were washed with PBS and 250 μL of 0.25% trypsin was added to each well. Once the cells were detached, the trypsin was neutralized with supplemented media. The RAECs were pelleted by centrifugation (600 × g) and resuspended in PBS. After the final wash, the PBS was aspirated, and the pellets (N=3) were dissolved in 6 mL of 2% nitric acid. The samples were measured with ICP-MS. Li, Y, and In were used as internal standards with a limit of detection of 6 ppb.

2.5. Measurement of reactive oxygen species

RAECs were exposed to 20 μg/mL of pristine, annealed, oxidized or reduced ZnO NPs from 15 min to 24 hrs. Presence of ROS was measured by H_2DCFDA. Following treatment, the cells were trypsinized, pelleted, washed 3× with PBS and resuspended in 2.5 μM of H_2DCFDA (Molecular Probes, OR, USA) and incubated for 30 min at 37 °C. Cellular fluorescence was measured with an Accuri C6 Flow Cytometer (BD Biosciences, San Jose, CA, USA). In addition, RAECs were pretreated with 1μM N-Acetylcysteine (NAC) in

supplemented media for 24 hrs and the medium was replaced before adding the ZnO NPs. The cells were exposed to pristine, annealed, oxidized or reduced ZnO NPs for different durations (15 mins to 24 hrs) and ROS was measured by H_2DCFDA.

RAEC were cultured on coverslips coated with gelatin for visual assessment of oxidative stress. Cell, were exposed to ZnO NPs (20 μg/ml) for 1hr and were treated with CellRox® (5 μM), Molecular Probes) for 30 min and fixed with 4% formaldehyde. Nuclei of the cells were stained with Hoescht 33362 trihydrochloride trihydrate. Images were recorded using a Nikon A1 laser scanning confocal microscope with an excitation of 405 and 488nm (N=2).

2.6. Measurement and ZnO nanoparticle reactivity with glutathione

RAECs were exposed to 20 μg/mL of pristine, annealed, oxidized or reduced ZnO NPs for 6, 12, and 24 h. The cell fraction was collected and prepared for high pressure liquid chromatography (HPLC) measurements of the thiol/disulfide couples concentrations to determine the cellular redox potential. The procedures were based on that of Jones et al (Jones and Liang, 2009). Briefly, the cell pellet was resuspended in 0.5 mL of 5% perchloric acid (PCA)/0.2 M boric acid/10 μM ϒ-Glu-Cys and then sonicated. Samples were centrifuged at 13000 × g for 2 min and 300 μl of the supernatant was placed in a new tube. The tubes with the pellets were aspirated and stored for protein quantification by bicinchoninic acid (BCA) protein assay. Derivation of samples to extract the thiol/disulfide couples was performed on the collected supernatant. For each sample, 60 μL of 9.3 mg/mL iodoacetic acid was added, and the pH was adjusted to 8.8 to 9.2 with 1M KOH. The samples were incubated for 20 min at room temperature after which 300 μl of 20 mg/mL of dansyl chloride was added to each sample. The samples were placed in the dark overnight. For each sample, 500 μL of chloroform was added, vortexed, and centrifuged at 13,000 × g for 2 min to separate the aqueous and organic layers. HPLC was performed on an amino column with a Supelcosil™ LC-NH2 25 cm × 4.6 mm, 5 μm column (Supleco, Bellefonte, PA, USA) with an Agilent 1200 HPLC equipped with a fluorimeter. The concentration of glutathione, its disulfide form GSSG, cysteine (Cys), and cystine (CySS) was determined from the scans. The Nernst equation was used to calculate the redox potential of the thiol/disulfide ratio (eq 1)

$$E_h(mV) = E_0 + (RT/nF)\ln([\text{acceptor}]/[\text{donor}]) \quad (1)$$

E_h: redox potential

E_0: standard potential at a defined pH

R: universal gas constant

T: absolute temperature (K)

F: Faraday's constant

n: number of electrons transferred

Assessment of ZnO NPs free thiol reactivity was measured using an Elman's assay. ZnO NPs with and without chemical defects were incubated with reduced L-glutathione (GSH) at 37 °C for 30min. Using Elman's reagent (5,5-dithio-bis-(2-nitrobenzoic acid). Measurements at 412nm and a molar coefficient of 14,150 m/cm was used to calculate the concentration of free thiols. Cyclic voltammetry was used to ascertain the charge transfer between glutathione and ZnO NPs. A three electrode setup with Ag/AgCl as a reference electrode, platinum wire as the auxillary/counter electrode, and various ZnO NPs as the working electrode. Glutathione solution (1 mM) in PBS was used as an electrolyte to study the charge transfer and pure PBS as a control. ZnO NPs were immobilized on a glassy carbon working electrode and tested in the glutathione solution.

2.7. Western blot analysis of ER stress pathways

PERK, pPERK, IRE, CHOP, pJNK, BIP, and Caspase-3 antibodies were purchased from Cell Signaling Technology® (Danvars, MA). GCLC, pIRE, ATF6 (90 kd) and diluted to a concentration of 1:1000, and XBP1 antibodies were purchased from Abcam Biotechnology and was used at 2 μg/ml (Cambridge, MA). Actin antibody was purchased from Sigma Aldrich (St. Louis, MO). The RAECs were exposed to pristine, annealed, oxidized or reduced ZnO NPs (20 μg/mL) for 6, 12, and 24 h in 100 mm dishes. The cells were washed with cold PBS, scraped, and pelleted. The pellets were lysed with 1% SDS and 80 mM Tris HCl containing protease and phosphatase inhibitor cocktails purchased from Sigma Aldrich (Sigma Aldrich, St. Louis, MO, USA). Samples were loaded into 12% tris-glycine gels (Thermo Fisher Scientific, MO, USA) to separate the proteins based on their size. The membranes were probed using antibodies listed above and exposed to goat anti-mouse or goat anti-rabbit secondary antibodies purchased from LiCor Biosciences and imaged using an Odyssey Infrared Imaging System (NE, USA). ImageJ software (NIH) was used for densiometric analysis and normalized with the corresponding actin band.

2.8. Transmission Electron Microscopy

Rat aortic endothelial cells were grown on sapphire discs in complete media and before treatment the cells were washed with unsupplemented DMEM/F12 media. Cells were exposed to silver nanoparticles at a concentration of 20 μg/ml for 3 hrs then were high pressure frozen using a Wohlwend Compact 02 high pressure freezer (Technotrade International, Manchester, NH). Frozen specimens were then freeze-substituted in anhydrous acetone containing 2% osmium tetroxide and 0.2% uranyl acetate and embedded in Epon/Araldite resin. Serial thin sections (80 nm) were cut using a Leica UCT ultramicrotome. Serial sections were collected on Formvar-coated copper slot grids, poststained with 2% aqueous uranyl acetate followed by Reynold's lead citrate and imaged using a Tecnai T12 Spirit TEM, operating at 100 kV.

2.9. Statistical analysis

Data are presented as the means ± standard error of means with sample size of n=3 for each group and all experiments were repeated at least three times. The numerical results were analyzed using one-way ANOVA with Dunnet's post-hoc analysis to determine statistical differences. A Pearson correlation was used to determine correlations between defects and

cellular toxicity. A P value <0.05 was considered to be statistically significant. All data were analyzed with Graphpad PRISM® (Version 5.01).

3. Results

3.1 Nanoparticle characterization

Pristine, annealed, oxidized and reduced ZnO NPs were characterized using transmission electron microscopy (TEM) and dynamic light scattering (DLS) to measure both their dehydrated and hydrodynamic diameter in water and DMEM/F12 cell culture media (Supplemental Figure 1 and Table 1). The zeta potential (mV) was measured in deionized water and DMEM (Table 1). The hydrodynamic size of pristine ZnO NPs was 213.4 nm and the size of the annealed, oxidized and reduced ZnO NPs were similar at 224.6 nm, 230.1 nm, and 200.7 nm respectively. The hydrodynamic size was ~4–5 times larger than the size obtained from TEM suggesting that all samples exhibited similar agglomeration. Furthermore, similar levels of ZnO NP agglomeration were also observed in DMEM/F12 media (Table 1). All the ZnO NPs showed Zincite crystal structure in x-ray diffraction (Supplemental Figure 2a).

X-ray photoelectron spectroscopy (XPS) was used to determine the stoichiometry of all ZnO NPs (Figure 1a). In XPS, the number of electrons ejected is recorded when sample surface is irradiated by X-rays. Given that different electrons in each atom are different in a binary compound such as ZnO, the stoichiometry could be determined based on the intensity of electrons ejected from different orbitals. In the case of Zn, we used 2p-orbital energies while 1s orbitals were used for O. The Zn 2p core-level in the XPS spectrum for all ZnO NPs showed two distinct peaks ~1021 and 1044 eV that likely attributed to Zn $2p_{3/2}$ and Zn $2p_{3/2}$, respectively (Zheng, Jiang and Lian, 2011, Moulder, 1992, Das, Pradhan, Sahu, Mishra, Sarangi, Nayak, Verma and Roul, 2010). On the other hand, O 1s exhibited two peaks at 530.5 and 532 eV, which arise from Zn–O bonding in ZnO and C=O peak from the surface adsorbed acetate from the decomposition of zinc acetate during the synthesis. Based on XPS analysis, the ratio of O/Zn was found to be different in different samples (Figure 1a). While pristine samples showed Zn/O ratio of ~0.92, annealed samples displayed better stoichiometry with ~0.96. The oxidized and reduced samples showed off-stoichiometry with Zn/O ratio ~0.85 and ~0.61. The off-stoichiometry may primarily be attributed the presence of Zn vacancies (V_{Zn}) and anti-sites (O_{Zn}), which can result in new electronic states within the band gap (see Supplemental Figure 3). We ruled out O interstitials due to the large size of O atoms compared ZnO unit cell. Furthermore, we found that annealing oxidized and reduced ZnO NPs in Zn vapors led to original stoichiometry (0.91 and 0.85) suggesting that the defects are mostly Zn vacancies.

In the case of direct band gap materials, illumination with light above the band gap energy results in fluorescence at the band gap. In regards to ZnO, it is known that an extra fluorescent band appears in the green-yellow region due to the presence of defects. Accordingly, the band gap and defect emission of pristine, annealed, oxidized and reduced ZnO NPs were measured by photoluminescence (PL) (Figure 1b) (Egblewogbe, Anand, Podila, Philip, Siva Sankara Sai and M. Rao, 2012). The band gap for all the samples was found to be the same, ~3.23 eV, indicating that E_C and E_V of our samples were not changed

due to the treatment. The presence of defects in ZnO NPs is known to result in green-yellow emission, as described in (Egblewogbe, Anand, Podila, Philip, Siva Sankara Sai and M. Rao, 2012, Reshchikov, Morkoç, Nemeth, Nause, Xie, Hertog and Osinsky, 2007). All the PL spectra were normalized to the band gap intensity to compare the defect densities across samples. As seen in Figure 1b, oxidized and reduced ZnO NPs showed the highest intensity for the defect emission, while pristine and annealed had a lower normalized intensity, which concurs with XPS studies. Together, PL and XPS results revealed that pristine and annealed samples had nearly ideal stoichiometry (~0.92 and ~0.96) with a less intense defect emission peak while oxidized and reduced samples were off-stoichiometric (~0.85 and 0.61) with highly intense defect-emission peaks. In addition to photoluminescence studies, we also performed non-linear optical studies to confirm the presence of defect-induced electronic states (Egblewogbe, Anand, Podila, Philip, Sai and Rao, 2012). Specifically, we measured the three-photon absorption coefficient (γ) for different ZnO NPs as a function of different excitation intensities (I_o) at 1064 nm using a Z-scan method. As described in Egblewogbe *et al.* and Podila *et al.*, the measured variation γ with I_0 is a direct indicator for the presence of defect-induced electronic states within the band gap (Supplemental Figure 2b) (Egblewogbe, Anand, Podila, Philip, Sai and Rao, 2012, Podila, Anand, West, Philip, Sai, He, Skove, Hwu, Tewari and Rao, 2011).

The percentage dissolution and average dissolved concentration was captured for the ZnO NPs under biologically relevant media over a period of 24 hours (as shown in Figure 2). The maximum dissolution for all nanostructures was observed in the case of artificial lysosomal fluid (pH~ 4.5) followed by cell culture media (DMEM) and least in the case of de-ionized water. Based on Gibbs Thompson equation, aggregation in a nanosystem has its knock on effect on the formation of concave curvatures (thermodynamically favorable) that lowers the equilibrium solubility which is contrary in the case of highly dissolving systems, this effect is prominent with the variation in the wetted surface area under dynamic conditions (Borm, Klaessig, Landry, Moudgil, Pauluhn, Thomas, Trottier and Wood, 2006, Kaptay, 2012, Paruthi, Rajput and Misra, 2019). The recovery of Zn^{2+} ions across 3.5 kDa membrane in DMEM and ALF was experimentally evaluated as 96.91% and 98.08% respectively. The rate constant is computed by employing Noyes Whitney equation on the dissolution profiles:

$$y(t) = y_0\left(1 - e^{-kt}\right) \quad \text{(Eq.2)}$$

where: y(t)= amount of dissolution of nanoparticle from the surface; y_0 = steady state concentration of released ionic species into the bulk solution; k= dissolution rate constant; t=time(hours). The rate of dissolution under all media conditions was computed. It was found to be minimum for pristine ZnO NPs (elaborated in table 2). Importantly, in DMEM media, the dissolution rate was similar across the 4 ZnO NP types.

3.2. ZnO nanoparticles reduce cell viability by induction of apoptosis

Vascular endothelial cells line the interior of blood vessels and are quickly exposed to NPs which have entered the circulatory system. Therefore, in this study we utilized rat aortic endothelial cells (RAECs) as an *in vitro* model to investigate the impact of NPs on the vascular system. The cellular viability of RAECs was measured by MTS assay at 24 and 48

hrs following exposure to 0, 5, 10, 15, 20 or 25 μg/mL of pristine, annealed, oxidized or reduced ZnO NPs (Figure 3a and Supplemental Figure 4). There was a significant reduction in viability of RAECs at all concentrations of annealed, oxidized and reduced ZnO NPs after a 24 h exposure, while pristine ZnO NPs reduced viability only with the 15, 20, and 25 μg/ml concentrations. Based on ZnO pristine NP toxicity range (15–25 μg/ml) 20 μg/ml was chosen for further investigation into the mechanism(s) of toxicity related to chemical defects. Annexin/PI staining of RAECs exposed to ZnO NPs for 24 hrs indicated a significant increase in the percentage of apoptotic cells (Figures 3b & c). Importantly, apoptosis was significantly increased in cells exposed to ZnO NPs with chemical defects (oxidized and reduced samples which were highly off-stoichiometric containing defects) compared to pristine ZnO NPs (Figure 3b). For further experiments to assess oxidative and ER stress, 20 μg/ml was chosen as a concentration of ZnO NPs which appears to induce cell apoptosis at 24 hrs, but at which ~75% of cells remain viable. In addition, we focused on earlier time points (i.e. 3 hrs following exposure) to examine early mechanisms by which ZnO NPs may induce cell stress and toxicity. Lastly, we performed correlation analysis between cell viability and defect-induced photoluminescence (PL) intensities (from Figure 1b) for different ZnO NP concentrations (5, 15, and 25 ug/ml). The Pearson correlation coefficients were found to be −0.6, −0.67, and −0.53 respectively which suggest that there is a strong negative correlation between defect density (indicated by PL intensity) and cell viability (i.e., the lower the defects the more viable are the cells).

3.3. Cellular uptake of ZnO nanoparticles and production of reactive oxygen species

To begin examining mechanisms associated with the observed differences in cell viability, we first assessed cellular uptake and production of reactive oxygen species in RAECs exposed to 20 μg/mL of each type of ZnO NP for 3 hrs. For pristine, annealed, oxidized and reduced ZnO NPs, the cellular uptake was found to be 2.68 μg/ml, 3.01 μg/ml, 1.87 μg/ml, and 1.34 μg/ml by ICP-MS respectively (Figure 4a). There was a significant decrease in the cellular uptake of the oxidized and reduced ZnO NPs, with highly off-stoichiometric ratios (see Figure 1a), compared to that of pristine ZnO NPs. Annealed ZnO NPs had the highest uptake by RAECs but was not statistically different from pristine ZnO NPs (Figure 4a), which agrees with XPS and PL results that showed these samples to have similar stoichiometry with few defects. To confirm cellular uptake of ZnO NPs we used transmission electron microscopy and show in Supplemental Figure 5 that all four ZnO NP types were taken up in RAECs at 3 hr following exposure.

The conversion of H_2DCFDA to DCF in RAECs after exposure to 20 μg/mL of ZnO NPs for 15 min to 24 h was used as an indicator of reactive oxygen species production. Compared to untreated RAECs, we observed a biphasic increase in ROS production for all ZnO NP types which peaked at early time points (15–45 min) and was followed by a subsequent increase in ROS around 6 h (Figure 4b). Differences in ROS production was observed among the four ZnO NP types. At 6 h, there was a significantly higher increase in ROS production in the RAECs exposed to oxidized ZnO NPs, while the other ZnO NP types did not significantly increase ROS production. This effect is intriguing because oxidized samples showed high ROS despite having the lowest cellular uptake. This suggests that the defects-induced by oxidation possibly introduce O/Zn anti-sites (O_{Zn}) (evident from off-stoichiometry in Figure

1a) that in turn results in new electronic states within the band gap of ZnO (see supplementary Figure 3) that overlap with intracellular redox potential (IRP) unlike other samples. Lastly, confocal imaging using CellRox® staining of RAECs following treatment with ZnO NPs indicated an increase of ROS in cells incubated with annealed and oxidized particles (Supplementary Figure 6).

3.4. ZnO nanoparticles differentially induce endoplasmic reticulum stress

We next investigated if exposure to the various ZnO NPs will induce an ER stress response in RAECs. RAECs were exposed to 20 μg/mL of pristine, annealed, oxidized or reduced ZnO NPs for 6, 12, and 24 hrs and we examined the phosphorylation of IREα and PERK and expression of ATF6 as indicators of ER stress (Figure 5). The PERK pathway was the primary ER stress pathway induced by ZnO NPs (Figure 5). All four ZnO NP types increased pPERK/PERK after 12 h of exposure, however, we observed the greatest degree of PERK phosphorylation with the oxidized ZnO NPs followed by reduced and annealed ZnO NPs. While an increase in pPERK was observed at 6 and 24 h, the pPERK/PERK ratio was not significantly different among the four types of ZnO NPs (Figure 5). In addition to pPERK, we observed a minor increase in pIRE after 6 h exposure to annealed ZnO NPs. The expression of ATF6 was not significantly changed following exposure to ZnO NPs at 6, 12, and 24 h. Similarly, there was no significant difference in the level of expression of pJNK or XBP-1s, CHOP, BOP or Caspase 12 in RAECs following ZnO NP exposure.

3.5. ZnO nanoparticles differentially modulate glutathione redox potential

To investigate the impact of ZnO NPs on cellular redox status of RAECs, we measured the thiol/disulfide ratios, calculated redox potentials of intracellular GSH, assessed direct reduction of GSH by ZnO NPs and examined charge transfer from ZnO NPs to GSH. RAECs were exposed to 20 μg/mL of pristine, annealed, oxidized or reduced ZnO NPs for 6, 12, and 24 hrs and the concentrations of reduced glutathione (GSH) and oxidized glutathione (GSSG) were measured via HPLC. There was significant reduction (more negative potential) in the GSH redox potential of the RAECs exposed to annealed, oxidized and reduced ZnO NPs (Figure 6a–c). Additionally, no significant change in the cellular GSH redox potential was observed in RAECs exposed to pristine ZnO NPs. Further, direct reduction of GSH by ZnO NPs was observed in a cell-free assay and was most prominent with oxidized ZnO NPs (Figure 6D). Lastly, cyclic voltammetry indicated differences in the charge transfer between GSH and the various ZnO NPs (Figure 6e). Importantly, increased charge transfer to GSH was observed at the greatest from reduced and oxidized ZnO NPs (Figure 6e).

4. Discussion

In this study, we have prepared pristine and defected ZnO nanoparticles (NPs) (oxidized, reduced and annealed) and assessed three major cellular outcomes associated with NP exposure: 1) cytotoxicity/apoptosis; 2) reactive oxygen species production and oxidative stress; 3) endoplasmic reticulum stress. We intentionally prepared ZnO NPs under different environments to induce a variety of defects that would in turn result in new electronic states within the band gap. We hypothesized that the introduction of defect-induced electronic

states into ZnO NPs elicits new toxicological changes beyond the present theoretical frameworks. Overall, the results demonstrate that the presence of chemical defects due to synthesis in either a reducing or oxidizing environment significantly influences the toxicity of ZnO NPs. We observed an increase in apoptosis in endothelial cells exposed to oxidized or reduced ZnO NPs as compared to pristine ZnO NPs. In addition, we observed a decrease in the redox potential of glutathione and induction of ER stress that was greater with exposure to reduced or oxidized ZnO NPs as compared to pristine ZnO NPs. Importantly, the observed differences in cellular viability, ROS production, and redox potential cannot be fully attributed to differences in cellular uptake or ionic dissolution. While the pristine and annealed ZnO NPs were more readily taken up by endothelial cells, these conditions elicited the least amount of cellular stress and toxicity. In contrast, there was significantly less uptake of oxidized and reduced ZnO NPs, yet these elicited the greatest amount of cellular stress. Likewise, ionic dissolution cannot fully explain cellular stress and toxicity as we observed similar rates of Zn-ion dissolution across NP types in cell culture media and it appears from the TEM studies that the ZnO NPs remain in a particle form following uptake. Therefore, these overall results suggest that defect-induced electronic states in ZnO NPs in part contribute to the observed toxicological changes in rat aortic endothelial cells.

The physicochemical properties of NPs have been extensively studied for their contribution to toxicity in cells and animal models (Aillon, Xie, El-Gendy, Berkland and Forrest, 2009, Podila and Brown Jared, 2012). These properties include size, shape, charge, surface properties, dissolution, and band gap. For example, it has been shown that the structural defects in multiwalled carbon nanotubes contribute to lung toxicity (Fenoglio, Greco, Tomatis, Muller, Raymundo-Pinero, Beguin, Fonseca, Nagy, Lison and Fubini, 2008, Muller, Huaux, Fonseca, Nagy, Moreau, Delos, Raymundo-Pinero, Beguin, Kirsch-Volders, Fenoglio, Fubini and Lison, 2008). The band gap (energy between valence (E_V) and conduction (E_C)) is another physicochemical property that has been studied for its ability to induce oxidative stress particularly if the band gap overlaps with the intracellular redox potential (IRP) of the cell. It has been hypothesized that the electronic states of materials may result in the transfer of electrons between materials and cellular components which govern the cellular redox state (Zhang, Ji, Xia, Meng, Low-Kam, Liu, Pokhrel, Lin, Wang, Liao, Wang, Li, Rallo, Damoiseaux, Telesca, Mädler, Cohen, Zink and Nel, 2012). Zhang *et al.* reported that metal oxides can be hazard ranked based upon their band gap when it overlaps with the overall IRP of cells (Zhang, Ji, Xia, Meng, Low-Kam, Liu, Pokhrel, Lin, Wang, Liao, Wang, Li, Rallo, Damoiseaux, Telesca, Mädler, Cohen, Zink and Nel, 2012). However, it was noted that ZnO NPs are above the band gap range defined by Zhang et al. and do not fall within the metal oxide ranking of toxicity, but can still induce oxidative stress and toxicity (Zhang, Ji, Xia, Meng, Low-Kam, Liu, Pokhrel, Lin, Wang, Liao, Wang, Li, Rallo, Damoiseaux, Telesca, Mädler, Cohen, Zink and Nel, 2012). Further, there is conflicting data in the literature on the toxicity of ZnO NPs with some studies reporting non-toxic effects, further ZnO is listed as a material which is generally regarded as safe by the FDA (FDA, CFR Title 21, volume 3, Section. 182.8991), while others have reported toxicity in cells and animal models (Chen, Huo, Shi, Bai, Zhang, Zhao, Chang and Chen, 2014, Reddy, Feris, Bell, Wingett, Hanley and Punnoose, 2007, Adamcakova-Dodd, Stebounova,

Kim, Vorrink, Ault, O'Shaughnessy, Grassian and Thorne, 2014, Ho, Wu, Chein, Chen and Cheng, 2011, Espitia, Otoni and Soares, 2016).

We first confirmed the presence of defects within our ZnO NPs. Our XPS and PL results suggest that O_{Zn} anti-sites and V_{Zn} vacancies are present in off-stoichiometric oxidized and reduced ZnO NPs suggesting Zn vacancies or anti-sites, while pristine and annealed NPs showed near ideal stoichiometry. In addition, rates of ionic dissolution were similar across ZnO NP types in cell culture media. To determine the toxicity of our defected ZnO NPs, we first examined cellular uptake, ROS production and oxidative stress. As noted above, cellular uptake was greatest with pristine and annealed ZnO NPs, yet these NPs caused the least amount of cellular stress and toxicity in endothelial cells as compared to the oxidized and reduced ZnO NPs. The mechanism(s) driving differences in cellular uptake are unknown but are also possibly related to charge transfer and interaction with proteins within the cell culture media that facilitate uptake into the cells. We observed an acute increase in ROS across all ZnO NP types which was greatest in oxidized ZnO NPs at later time points. Further, we observed the greatest change in cellular redox potential with oxidized ZnO NPs despite the least amount of cellular uptake. Importantly, we also observed differences in the glutathione redox potential across particle types with exposure to the reduced and oxidized ZnO NPs resulting in the greatest reduction of glutathione as compared to pristine ZnO NPs. In addition, we observed direct reduction of glutathione in a cellular free assay as well as confirmed charge transfer between glutathione and ZnO NPs. While we have not elucidated the exact mechanisms associated with charge transfer, previous studies have shown proteins in the presence of a reducing agent affects their disulfide bonds, resulting in protein structural/conformational changes (Weichsel, Gasdaska, Powis and Montfort, 1996, Anfinsen and Haber, 1961, Logan, Su, Aberg, Regnstrom, Hajdu, Eklund and Nordlund, 1996, Mehta, Bee, Randolph and Carpenter, 2014). Moreover, organelles within cells have regulated redox potentials which depend on thiol/disulfide couples (Go and Jones, 2008). Importantly, our previous studies on ENM-protein corona formation demonstrated that physicochemical properties including alterations in surface functional groups influence protein conformational changes through charge transfer reactions between the NP and the protein (Shannahan, Lai, Ke, Podila, Brown and Witzmann, 2013, Raghavendra, Alsaleh, Brown and Podila, 2017, Podila, Chen, Ke, Brown and Rao, 2012, Podila, Vedantam, Ke, Brown and Rao, 2012).

Expanding on this discussion of charge transfer, Burello and Worth proposed that electrons could be transferred between engineered nanomaterials (ENMs) and cellular redox species depending upon the electronegativity, ionization potential, or semiconductor band gap energy between valence (E_V) and conduction (E_C) bands (Burello and Worth, 2011). In this model, the electron transfer occurs only when the molecular energy levels of cellular redox species (as gauged by intracellular redox potential or IRP) overlap with ENM energy bands (viz., E_C or E_V), which could ultimately produce reactive oxygen species (ROS) and reactive nitrogen species (RNS) on the ENM surface. This model was further ratified experimentally by Zhang et al (Zhang, Ji, Xia, Meng, Low-Kam, Liu, Pokhrel, Lin, Wang, Liao, Wang, Li, Rallo, Damoiseaux, Telesca, Mädler, Cohen, Zink and Nel, 2012). In the presence of defects (the presence of which is ratified by multiple spectroscopic techniques including XPS, PL, and Non-linear optical spectroscopy), there are new defect-induced electronic states between

E_c and E_V that could also contribute to electron transfer with cellular redox species, which could increase adverse responses. Thus, our results further generalize Burello and Worth's model by incorporating defect-induced electronic states. However, further work is needed to determine how changes in chemical defects within the structural lattice of a NP may influence cellular redox status through charge transfer reactions likely leading to changes in protein structure and function via thiol modifications.

In addition to ROS and glutathione redox potential, we examined ER stress in endothelial cells exposed to the defected ZnO NPs. Our results demonstrated that the ZnO NPs induce ER stress primarily through the PERK pathway possibly suggesting there is an accumulation of misfolded proteins likely from the increase in ROS production after exposure to ZnO NPs. Prior studies have indicated that ZnO NPs induce ER stress resulting in cell death (Chen, Huo, Shi, Bai, Zhang, Zhao, Chang and Chen, 2014). For example, Chen *et al.* have shown that exposing human umbilical vein endothelial cells (HUVEC) to ZnO NPs results in the induction of apoptosis (Chen, Huo, Shi, Bai, Zhang, Zhao, Chang and Chen, 2014). *In vivo* studies in mice, which were orally gavaged with ZnO NPs, resulted in liver toxicity and the induction of ER stress through the PERK pathway (Yang, Shao, Liu, Gu, Shu, Mo, Chen, Zhang and Jiang, 2015). The results of our study indicate a similar activation of the PERK pathway. Importantly, the highest levels of PERK phosphorylation were observed for RAECs exposed to oxidized ZnO NPs. We hypothesize that a charge transfer from the ZnO NPs may affect protein structure, thus resulting in an unfolded protein response leading to ER stress. In fact, we have previously reported that charge transfer interactions between NPs and apolipoprotein results in conformational changes in the protein (Raghavendra, Alsaleh, Brown and Podila, 2017). Further supporting this notion, we have recently reported that protein corona formation on silver nanoparticles and subsequent protein misfolding contributes to ER stress in endothelial cells (Persaud, H Shannahan, Raghavendra, B Alsaleh, Podila and M Brown, 2018). Both of these findings, along with the current results, suggests that charge transfer from the ZnO NP may elicit protein structure or stability changes that could contribute to ER stress.

5. Conclusion

In conclusion, these findings indicate chemical defects present in ZnO NPs in part contribute to cellular stress and toxicity in endothelial cells. These data suggest that reduced and oxidized ZnO NPs result in a reduced cellular state, possibly through interaction with proteins which have undergone structural changes due to NP-protein charge interactions or ROS production. Importantly, this response varied in degree due to the type of ZnO NP chemical defects present with the highest response observed for the reduced and oxidized ZnO NPs. Taken together these results indicate that the physicochemical properties of chemical defects and electronic states should be considered as a new framework when investigating the toxicity of NPs.

Supplementary Material

Refer to Web version on PubMed Central for supplementary material.

Acknowledgements:

We would like to acknowledge Kristofer Fritz and Peter Harris for their assistance with the HPLC assay for the redox potential. Electron microscopy was done at the University of Colorado, Boulder EM Services Core Facility in the Department of MCD Biology, with the technical assistance of facility staff. This work was funded by the National Institute of Environmental Health Sciences R01 ES019311 (JMB).

References

Klingshirn C. 2007 ZnO: From basics towards applications. physica status solidi (b) 244:3027–3073.

Roth AP, Webb JB and Williams DF. 1982 Band-gap narrowing in heavily defect-doped ZnO. Physical Review B 25:7836–7839.

Hong T-K, Tripathy N, Son H-J, Ha K-T, Jeong H-S and Hahn Y-B. 2013 A comprehensive in vitro and in vivo study of ZnO nanoparticles toxicity. J Mater Chem B 1:2985–2992.

Zhang Y, Nayak TR, Hong H and Cai W. 2013 Biomedical Applications of Zinc Oxide Nanomaterials. Current molecular medicine 13:1633–1645. [PubMed: 24206130]

Djurisic AB, Leung YH, Tam KH, Hsu YF, Ding L, Ge WK, Zhong YC, Wong KS, Chan WK, Tam HL, Cheah KW, Kwok WM and Phillips DL. 2007 Defect emissions in ZnO nanostructures. Nanotechnology 18.

Raghavendra AJ, Gregory WE, Slonecki TJ, Dong Y, Persaud I, Brown JM, Bruce TF and Podila R. 2018 Three-photon imaging using defect-induced photoluminescence in biocompatible ZnO nanoparticles. International journal of nanomedicine 13:4283–4290. [PubMed: 30087560]

Smijs TG and Pavel S. 2011 Titanium dioxide and zinc oxide nanoparticles in sunscreens: focus on their safety and effectiveness. Nanotechnology, science and applications 4:95–112.

Vandebriel RJ and De Jong WH. 2012 A review of mammalian toxicity of ZnO nanoparticles. Nanotechnology, science and applications 5:61–71.

Yu KN, Yoon TJ, Minai-Tehrani A, Kim JE, Park SJ, Jeong MS, Ha SW, Lee JK, Kim JS and Cho MH. 2013 Zinc oxide nanoparticle induced autophagic cell death and mitochondrial damage via reactive oxygen species generation. Toxicol In Vitro 27:1187–1195. [PubMed: 23458966]

Sharma V, Singh P, Pandey AK and Dhawan A. 2012 Induction of oxidative stress, DNA damage and apoptosis in mouse liver after sub-acute oral exposure to zinc oxide nanoparticles. Mutat Res 745:84–91. [PubMed: 22198329]

Zhang H, Ji Z, Xia T, Meng H, Low-Kam C, Liu R, Pokhrel S, Lin S, Wang X, Liao Y-P, Wang M, Li L, Rallo R, Damoiseaux R, Telesca D, Mädler L, Cohen Y, Zink JI and Nel AE. 2012 Use of Metal Oxide Nanoparticle Band Gap To Develop a Predictive Paradigm for Oxidative Stress and Acute Pulmonary Inflammation. ACS Nano 6:4349–4368. [PubMed: 22502734]

Xia T, Zhao Y, Sager T, George S, Pokhrel S, Li N, Schoenfeld D, Meng H, Lin S, Wang X, Wang M, Ji Z, Zink JI, Madler L, Castranova V, Lin S and Nel AE. 2011 Decreased dissolution of ZnO by iron doping yields nanoparticles with reduced toxicity in the rodent lung and zebrafish embryos. ACS Nano 5:1223–1235. [PubMed: 21250651]

Warheit DB, Sayes CM and Reed KL. 2009 Nanoscale and Fine Zinc Oxide Particles: Can in Vitro Assays Accurately Forecast Lung Hazards following Inhalation Exposures? Environmental Science & Technology 43:7939–7945. [PubMed: 19921917]

Sayes CM, Reed KL and Warheit DB. 2007 Assessing toxicity of fine and nanoparticles: comparing in vitro measurements to in vivo pulmonary toxicity profiles. Toxicol Sci 97:163–180. [PubMed: 17301066]

Cho WS, Duffin R, Poland CA, Howie SE, MacNee W, Bradley M, Megson IL and Donaldson K. 2010 Metal oxide nanoparticles induce unique inflammatory footprints in the lung: important implications for nanoparticle testing. Environ Health Perspect 118:1699–1706. [PubMed: 20729176]

Cho WS, Duffin R, Poland CA, Duschl A, Oostingh GJ, Macnee W, Bradley M, Megson IL and Donaldson K. 2012 Differential pro-inflammatory effects of metal oxide nanoparticles and their soluble ions in vitro and in vivo; zinc and copper nanoparticles, but not their ions, recruit eosinophils to the lungs. Nanotoxicology 6:22–35. [PubMed: 21332300]

Meyer K, Rajanahalli P, Ahamed M, Rowe JJ and Hong Y. 2011 ZnO nanoparticles induce apoptosis in human dermal fibroblasts via p53 and p38 pathways. Toxicol In Vitro 25:1721–1726. [PubMed: 21903158]

Xia T, Kovochich M, Liong M, Madler L, Gilbert B, Shi H, Yeh JI, Zink JI and Nel AE. 2008 Comparison of the mechanism of toxicity of zinc oxide and cerium oxide nanoparticles based on dissolution and oxidative stress properties. ACS Nano 2:2121–2134. [PubMed: 19206459]

Chen R, Huo L, Shi X, Bai R, Zhang Z, Zhao Y, Chang Y and Chen C. 2014 Endoplasmic Reticulum Stress Induced by Zinc Oxide Nanoparticles Is an Earlier Biomarker for Nanotoxicological Evaluation. ACS Nano 8:2562–2574. [PubMed: 24490819]

Yang X, Shao H, Liu W, Gu W, Shu X, Mo Y, Chen X, Zhang Q and Jiang M. 2015 Endoplasmic reticulum stress and oxidative stress are involved in ZnO nanoparticle-induced hepatotoxicity. Toxicol Lett 234:40–49. [PubMed: 25680694]

Puzyn T, Rasulev B, Gajewicz A, Hu X, Dasari TP, Michalkova A, Hwang HM, Toropov A, Leszczynska D and Leszczynski J. 2011 Using nano-QSAR to predict the cytotoxicity of metal oxide nanoparticles. Nature nanotechnology 6:175–178.

Burello E and Worth AP. 2011 A theoretical framework for predicting the oxidative stress potential of oxide nanoparticles. Nanotoxicology 5:228–235. [PubMed: 21609138]

Shannahan JH, Lai X, Ke PC, Podila R, Brown JM and Witzmann FA. 2013 Silver nanoparticle protein corona composition in cell culture media. PloS one 8:e74001. [PubMed: 24040142]

Podila R, Chen R, Ke PC, Brown JM and Rao AM. 2012 Effects of surface functional groups on the formation of nanoparticle-protein corona. Applied Physics Letters 101:263701. [PubMed: 23341687]

Podila R, Vedantam P, Ke PC, Brown JM and Rao AM. 2012 Evidence for Charge-Transfer-Induced Conformational Changes in Carbon Nanostructure–Protein Corona. The Journal of Physical Chemistry C 116:22098–22103.

Raghavendra AJ, Alsaleh N, Brown JM and Podila R. 2017 Charge-transfer interactions induce surface dependent conformational changes in apolipoprotein biocorona. Biointerphases 12:02D402.

Jones DP and Liang Y. 2009 Measuring the poise of thiol/disulfide couples in vivo. Free Radic Biol Med 47:1329–1338. [PubMed: 19715755]

Zheng JH, Jiang Q and Lian JS. 2011 Synthesis and optical properties of flower-like ZnO nanorods by thermal evaporation method. Applied Surface Science 257:5083–5087.

Moulder JF, Stickle WF, Sobol PE, Bomben KD and Chastain J. (1992). Handbook of X-Ray Photoelectron Spectroscopy: A Reference Book of Standard Spectra for Identification and Interpretation of XPS Data. Eden Prairie, MN; USA: Perkin-Elmer Corporation.

Das J, Pradhan SK, Sahu DR, Mishra DK, Sarangi SN, Nayak BB, Verma S and Roul BK. 2010 Micro-Raman and XPS studies of pure ZnO ceramics. Physica B: Condensed Matter 405:2492–2497.

Egblewogbe M, Anand B, Podila R, Philip R, Siva Sankara Sai S and Rao AM. (2012). Defect Induced Changes in the Linear and Non-Linear Optical Properties of ZnO Nanotetrapods.

Reshchikov MA, Morkoç H, Nemeth B, Nause J, Xie J, Hertog B and Osinsky A. 2007 Luminescence properties of defects in ZnO. Physica B: Condensed Matter 401–402:358–361.

Egblewogbe M, Anand B, Podila R, Philip R, Sai SSS and Rao AM. 2012 Defect Induced Changes in the Linear and Non-Linear Optical Properties of ZnO Nanotetrapods. Materials Express 2:351–356.

Podila R, Anand B, West JP, Philip R, Sai SS, He J, Skove M, Hwu SJ, Tewari S and Rao AM. 2011 Evidence for surface states in pristine and Co-doped ZnO nanostructures: magnetization and nonlinear optical studies. Nanotechnology 22:095703. [PubMed: 21258145]

Borm P, Klaessig FC, Landry TD, Moudgil B, Pauluhn J, Thomas K, Trottier R and Wood S. 2006 Research strategies for safety evaluation of nanomaterials, part V: role of dissolution in biological fate and effects of nanoscale particles. Toxicological sciences: an official journal of the Society of Toxicology 90:23–32. [PubMed: 16396841]

Kaptay G. 2012 On the size and shape dependence of the solubility of nano-particles in solutions. International journal of pharmaceutics 430:253–257. [PubMed: 22486956]

Paruthi A, Rajput V and Misra SK. 2019 Single platform spin-spin nuclear relaxation time (1H NMR) based technique for assessing dissolution and agglomeration of CuO nanoparticles. NanoImpact 14:100148.

Aillon KL, Xie Y, El-Gendy N, Berkland CJ and Forrest ML. 2009 Effects of nanomaterial physicochemical properties on in vivo toxicity. Advanced Drug Delivery Reviews 61:457–466. [PubMed: 19386275]

Podila R and Brown Jared M. 2012 Toxicity of Engineered Nanomaterials: A Physicochemical Perspective. Journal of Biochemical and Molecular Toxicology 27:50–55. [PubMed: 23129019]

Fenoglio I, Greco G, Tomatis M, Muller J, Raymundo-Pinero E, Beguin F, Fonseca A, Nagy JB, Lison D and Fubini B. 2008 Structural defects play a major role in the acute lung toxicity of multiwall carbon nanotubes: physicochemical aspects. Chemical research in toxicology 21:1690–1697. [PubMed: 18636755]

Muller J, Huaux F, Fonseca A, Nagy JB, Moreau N, Delos M, Raymundo-Pinero E, Beguin F, Kirsch-Volders M, Fenoglio I, Fubini B and Lison D. 2008 Structural defects play a major role in the acute lung toxicity of multiwall carbon nanotubes: toxicological aspects. Chemical research in toxicology 21:1698–1705. [PubMed: 18636756]

Reddy KM, Feris K, Bell J, Wingett DG, Hanley C and Punnoose A. 2007 Selective toxicity of zinc oxide nanoparticles to prokaryotic and eukaryotic systems. Applied physics letters 90:2139021–2139023. [PubMed: 18160973]

Adamcakova-Dodd A, Stebounova LV, Kim JS, Vorrink SU, Ault AP, O'Shaughnessy PT, Grassian VH and Thorne PS. 2014 Toxicity assessment of zinc oxide nanoparticles using sub-acute and sub-chronic murine inhalation models. Part Fibre Toxicol 11:15. [PubMed: 24684892]

Ho M, Wu KY, Chein HM, Chen LC and Cheng TJ. 2011 Pulmonary toxicity of inhaled nanoscale and fine zinc oxide particles: mass and surface area as an exposure metric. Inhal Toxicol 23:947–956. [PubMed: 22122307]

Espitia PJP, Otoni CG and Soares NFF. (2016). Chapter 34 - Zinc Oxide Nanoparticles for Food Packaging Applications In: Barros-Velázquez J ed. Antimicrobial Food Packaging. San Diego: Academic Press, 425–431.

Weichsel A, Gasdaska JR, Powis G and Montfort WR. 1996 Crystal structures of reduced, oxidized, and mutated human thioredoxins: evidence for a regulatory homodimer. Structure 4:735–751. [PubMed: 8805557]

Anfinsen CB and Haber E. 1961 Studies on the reduction and re-formation of protein disulfide bonds. J Biol Chem 236:1361–1363. [PubMed: 13683523]

Logan DT, Su XD, Aberg A, Regnstrom K, Hajdu J, Eklund H and Nordlund P. 1996 Crystal structure of reduced protein R2 of ribonucleotide reductase: the structural basis for oxygen activation at a dinuclear iron site. Structure 4:1053–1064. [PubMed: 8805591]

Mehta SB, Bee JS, Randolph TW and Carpenter JF. 2014 Partial Unfolding of a Monoclonal Antibody: Role of a Single Domain in Driving Protein Aggregation. Biochemistry 53:3367–3377. [PubMed: 24804773]

Go YM and Jones DP. 2008 Redox compartmentalization in eukaryotic cells. Biochim Biophys Acta 1780:1273–1290. [PubMed: 18267127]

Podila R, Chen R, Ke PC, Brown JM and Rao AM. 2012 Effects of surface functional groups on the formation of nanoparticle-protein corona. Appl Phys Lett 101:263701. [PubMed: 23341687]

Podila R, Vedantam P, Ke PC, Brown JM and Rao AM. 2012 Evidences For Charge Transfer-Induced Conformational Changes In Carbon Nanostructure-Protein Corona. J Phys Chem C Nanomater Interfaces 116:22098–22103. [PubMed: 23243478]

Persaud I, H Shannahan J, Raghavendra A, B Alsaleh N, Podila R and Brown JM. (2018). Biocorona formation contributes to silver nanoparticle induced endoplasmicreticulum stress.

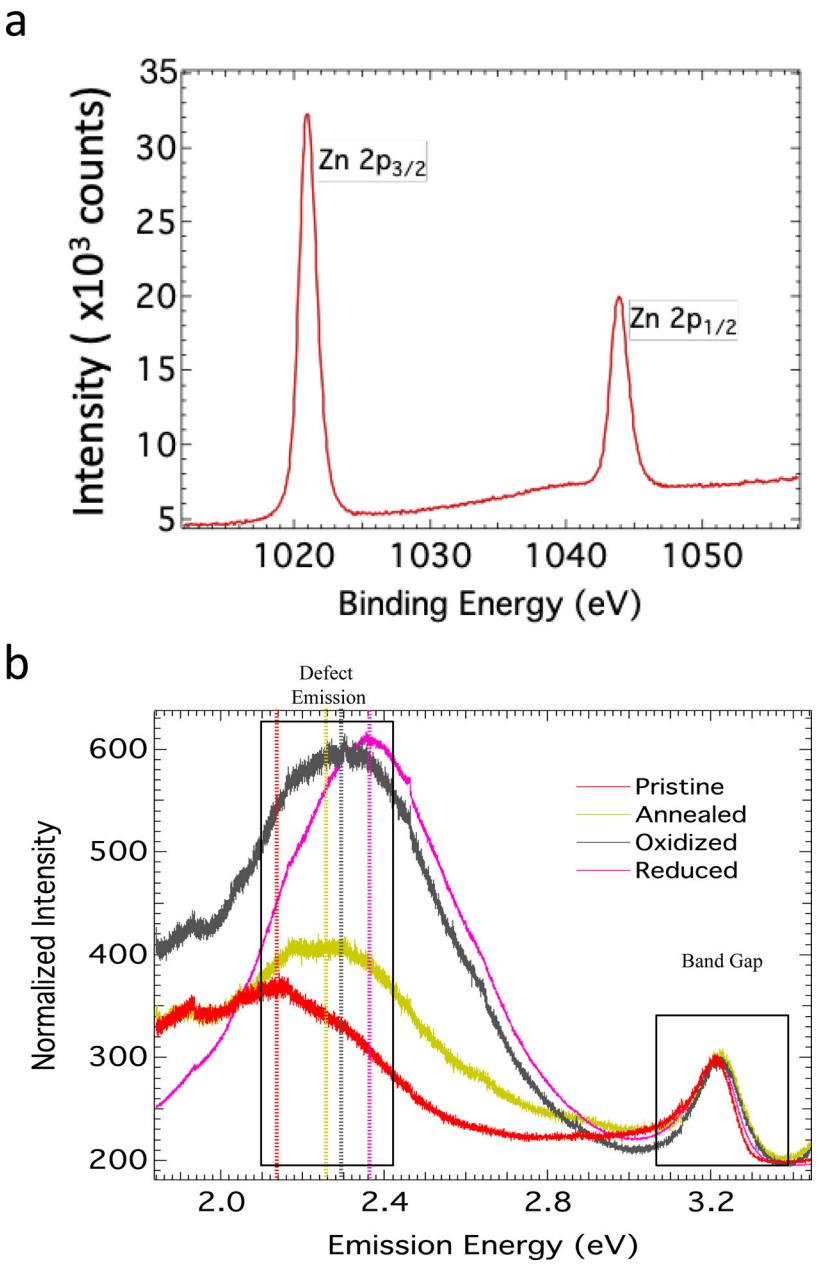

Figure 1: Defect and Band Gap Emissions of Pristine, Annealed, Oxidized, and Reduced ZnO Nanoparticles

Defects were analyzed using XPS (a) and PL (b) spectroscopy. The stoichiometric ratio of Zn/O are obtained from Zn and O XPS peaks (see the inset figure in 1a) as described in the text (see the table inset in figure 1a). The PL spectrum in (b) indicates the defect emission at an emission energy of 2.0 to 2.8. The band gap intensity is shown at an emission energy of 3.0 to 3.4.

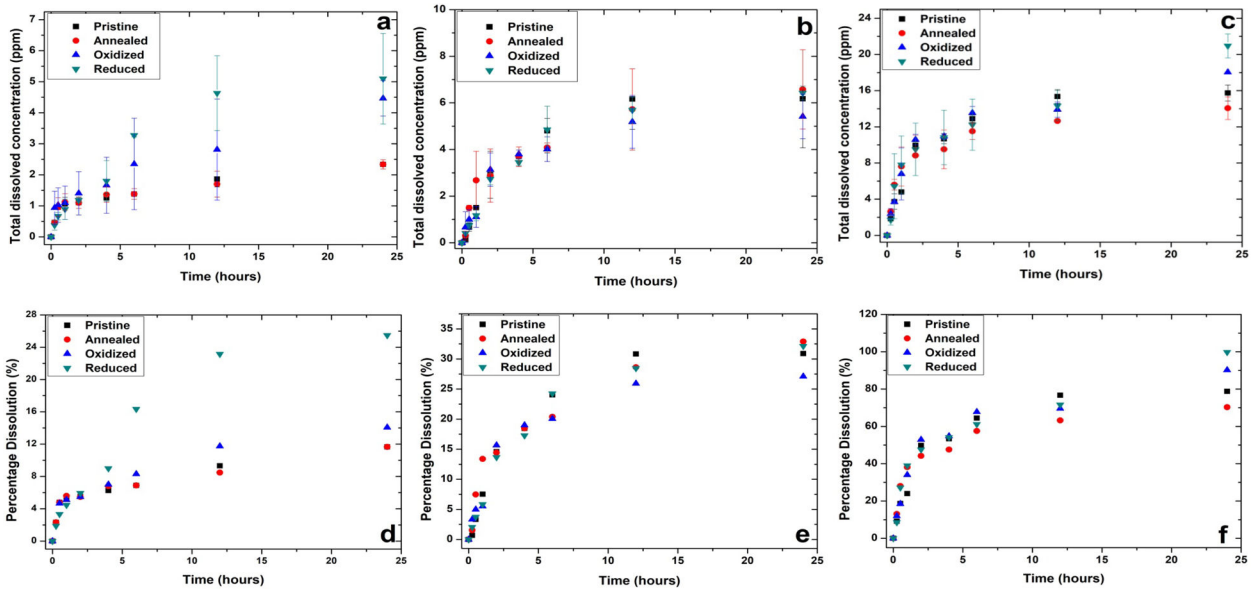

Figure 2:

Average dissolved concentration (ppm) of ZnO nanostructures suspended in (A) de-ionized water at 25°C, pH= 7.1±0.2 (B) cell culture media (DMEM) at 37°C and (C) artificial lysosomal fluid (ALF) at 37°C, pH= 4.3±0.4. Percentage dissolution of ZnO nanostructures in (D) de-ionized water, (E) cell culture media (DMEM) and (F) ALF over the period of 24 hours. The data is represented as mean ± standard error (n=2).

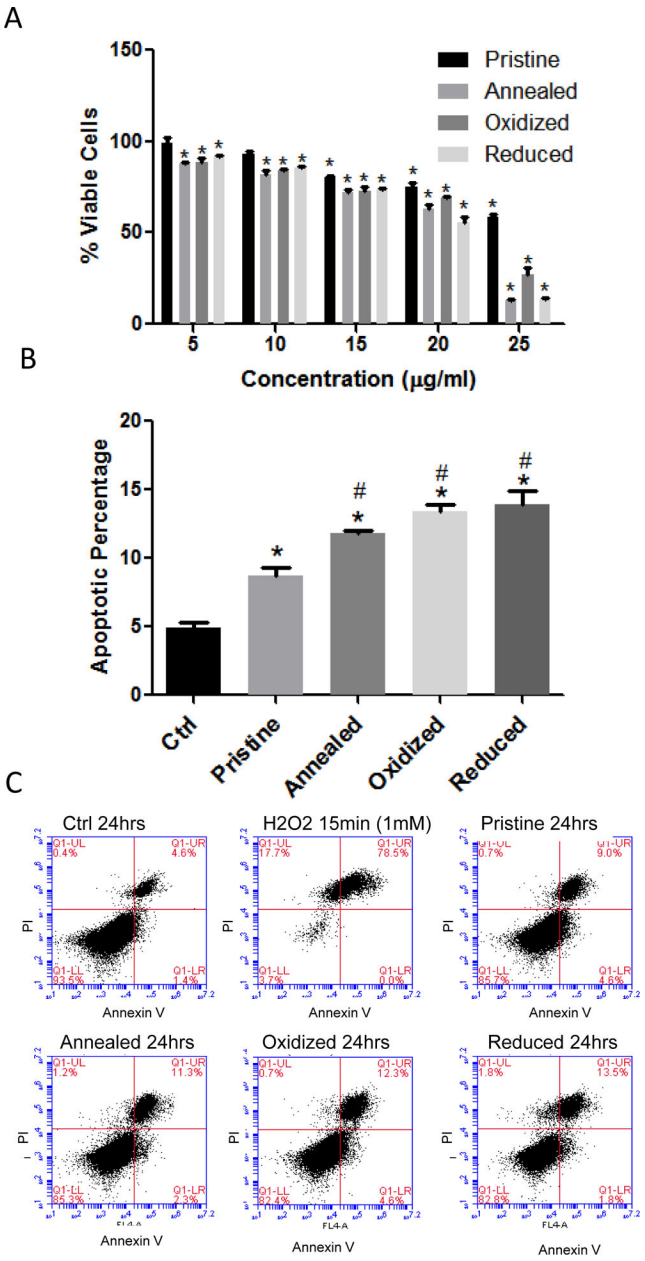

Figure 3: Cell Viability Measurements in Rat Aortic Endothelial Cells Exposed to ZnO Nanoparticles.

RAECs were exposed to pristine, annealed, oxidized or reduced ZnO NPs and analyzed for cell viability using MTS assay and Annexin V/PI staining. (A) For the MTS assay, RAECs were exposed to ZnO NPs for 24hrs at 5–25 µg/ml and cell viability was determined. *statistically significant compared to control (untreated cells) ($P<0.05$). (B) Annexin V/PI staining was used to determine apoptosis in RAECs exposed to ZnO NPs at 20 µg/ml for 24 hrs (N=3) (*statistically significant compared to control, #statistically significant compared to pristine ZnO NPs ($P<0.05$). (C) Representative flow cytometry plots of the Annexin/PI in RAEC exposed to ZnO NPs at 24 hrs. Hydrogen peroxide (1mM) was used as positive control.

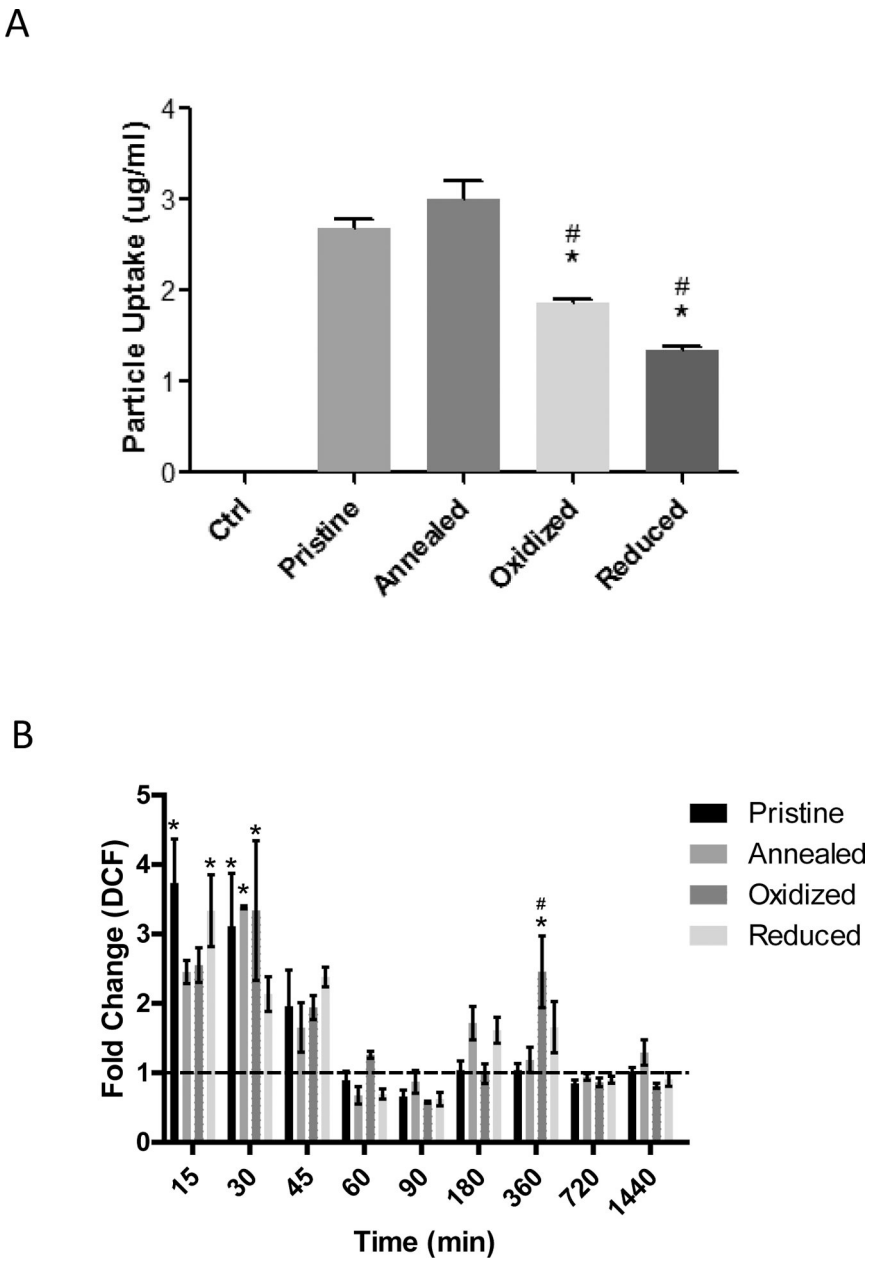

Figure 4: Rat Aortic Endothelial Cell Uptake of ZnO Nanoparticles and Reactive Oxygen Species Production.

(A) RAECs were exposed to 20 μg/ml of pristine, annealed, oxidized or reduced ZnO NPs and cellular uptake was measured using ICP-MS. (N=3) (B) Measurement of reactive oxygen species production as assessed by H_2DCFDA in RAECs exposed to ZnO NPs (20 μg/ml) (N=3). *statistically significant compared to pristine ZnO NPs, #statistically significant compared to annealed ZnO NPs ($P<0.05$).

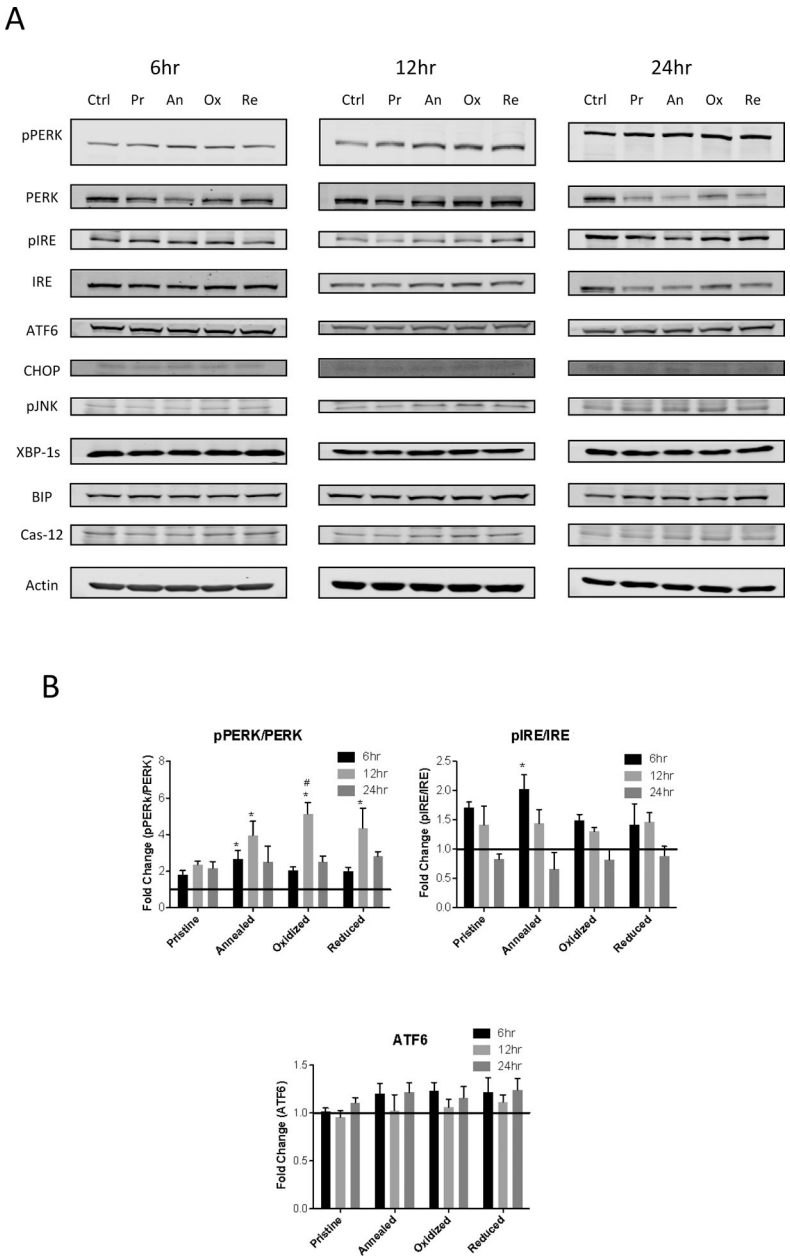

Figure 5: Western Blot Analysis of Endoplasmic Reticulum Stress Proteins in Rat Aortic Endothelial Cells Exposed to ZnO Nanoparticles:

RAECs were exposed to pristine, annealed, oxidized or reduced ZnO NPs. (A) Images of key ER stress proteins at 6, 12, and 24 hrs following exposure to ZnO NPs at 20 μg/ml. (B) Densiometric analysis of PERK, IRE and ATF6 protein expression (N=3). *statistically significant compared to control (untreated cells), #statistically significant compared to pristine ZnO NPs ($P<0.05$).

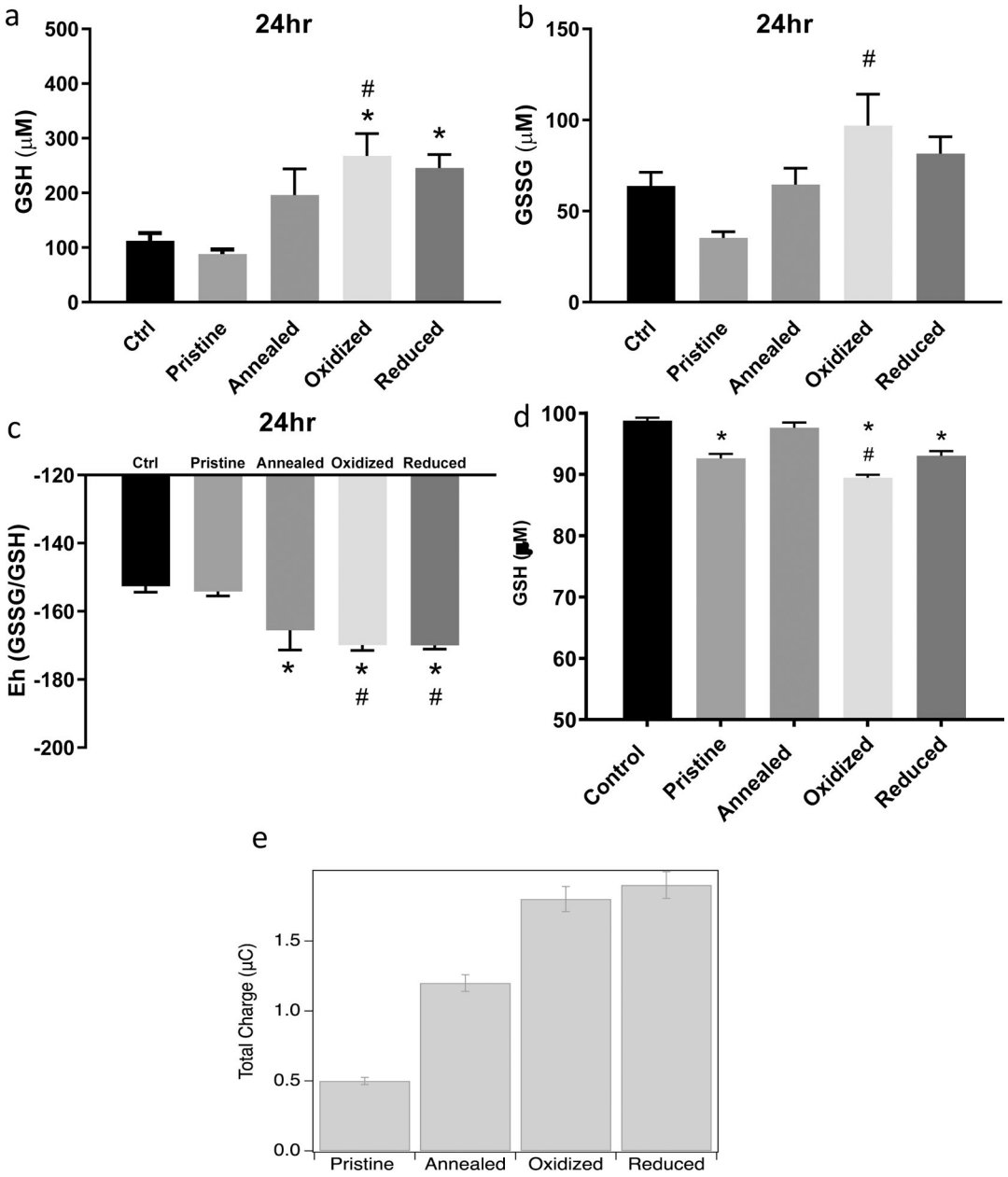

Figure 6: Glutathione Redox Potential Measurement in Rat Aortic Endothelial Cells Exposed to ZnO Nanoparticles and Charge Transfer.

RAECs were exposed to pristine, annealed, oxidized or reduced ZnO NPs for 24hrs at 20 μg/ml. Intracellular reduced and oxidized glutathione (GSH (A) and GSSG (B) respectively) concentrations were measured using HPLC (N=3). (C) The redox potential (E_h) was calculated using the Nernst equation ($E_h=E_0$ + (RT/nF)ln([acceptor]/[donor]). (D) Measurement of ZnO NPs direct reactivity with cell free GSH incubated for 15 min at 37 °C as measured by Elman's reagent. (E) ZnO NP cyclic voltammetry for the measurement of charge transfer between gluthathione and ZnO NPs. A three-electrode setup measured the charge transfer of ZnO (1 mg/ml) nanoparticles with and without chemical defects to

gluthathione (1mM). *statistically significant compared to control (untreated cells). #statistically significant compared to pristine ZnO NPs ($p<0.05$).

Table 1:

ZnO Nanoparticle Characterization.

Dynamic light scattering was utilized to measure nanoparticle hydrodynamic size, zeta potential and polydispersity index (PDI) in water and DMEM cell culture media; TEM was used to measure nanoparticle diameter (N=3).

	H_2O			DMEM			TEM
ZnO	**Hydrodynamic size (d.nm)**	**Zeta potential (mV)**	**PDI**	**Hydrodynamic size (d.nm)**	**Zeta potential (mV)**	**PDI**	**Particle Size (d.nm)**
Pristine	213.40 ± 12.10	35.2 ± 1.20	0.34 ± 0.03	279.80 ± 48.90	−14.00 ± 0.65	0.46 ± 0.07	37.00 ± 11.00
Annealed	224.60 ± 28.70	−16.97 ± 1.00	0.57 ± 0.10	209.60 ± 42.10	−7.96 ± 3.21	0.68 ± 0.10	57.00 ± 14.00
Oxidized	230.10 ± 11.10	18.40 ± 0.90	0.45 ± 0.03	197.70 ± 41.60	−9.67 ± 0.23	0.55 ± 0.10	57.00 ± 20.00
Reduced	200.70 ± 15.90	10.08 ± 0.60	0.71 ± 0.14	117.90 ± 67.30	−6.05 ± 0.21	0.92 ± 0.13	54.00 ± 16.00

Table 2:

Total dissolution quantification of ZnO nanostructures under biologically relevant media conditions

	Pristine		Annealed		Oxidized		Reduced	
	Rate (h^{-1})	% Dissolution	Rate (h^{-1})	% Dissolution	Rate (h^{-1})	% Dissolution	Rate (h^{-1})	% Dissolution
De-ionized Water	0.127	11.6±0.7	0.215	11.6±0.85	0.230	14.06±8.13	0.186	25.47±7.3
DMEM Cell Culture Media	0.476	30.8±10.5	0.521	32.8±8.5	2.98	27.09±4.7	3.92	32.1±1.4
Artificial Lysosomal Fluid (ALF)	1.613	78.7±4.4	1.516	70.3±6.2	1.77	90.2±0.2	1.78	99.78±6.6